Silica Microspheres with Adsorbed Gold Nanostars for Single Cell SERS Detection of Formazan

Olga A. Inozemtseva[1,2*], Ekaterina S. Prikhozhdenko[1], Olga I. Gusliakova[2], Yulia A. Tyunina[1,2], Mariia S. Saveleva[1], Daniil N. Bratashov[1], Andrey M. Burov[2], and Boris N. Khlebtsov[2]

[1] Saratov State University, 83 Astrakhanskaya str., Saratov 410012, Russian Federation

[2] Institute of Biochemistry and Physiology of Plants and Microorganisms of the Russian Academy of Sciences – a separate structural subdivision of the Federal State Budgetary Scientific Institution Federal Research Center "Saratov Scientific Center of the Russian Academy of Sciences", 13 Entuziastov ave., Saratov 410049, Russian Federation

[*]e-mail: Inozemtsevaoa@mail.ru

Abstract. In this study we report a rapid and sensitive surface-enhanced Raman spectroscopy (SERS)-based 3-(4, 5-dimethylthiazol-2-yl)-2,5-diphenyltetrazolium bromide (MTT) assay for *in situ* cell viability and proliferation assessment. The developed method based on silica microspheres with adsorbed gold nanostars serves as intracellular SERS platforms for formazan detection. The proposed method has several advantages over traditional MTT assays. Firstly, the formazan concentration can be determined from the SERS signal intensity without extraction and enrichment steps. Secondly, the SERS spectra of formazan can be directly obtained at the level of a single particle internalized by the cell. The SERS-MTT detection method is expected to avoid interference from background substances (such as residual MTT reagent, serum, exogenous drugs) in cell suspensions. Furthermore, the proposed approach not only simplifies the testing procedure, but it is also anticipated to provide more precise results when evaluating the effectiveness of cancer treatments compared to the conventional MTT method. © 2024 Journal of Biomedical Photonics & Engineering.

Keywords: 3-(4, 5-dimethylthiazol-2-yl)-2,5-diphenyltetrazolium bromide (MTT); surface-enhanced Raman spectroscopy (SERS); formazan; gold nanostars.

Paper #9160 received 30 Aug 2024; revised manuscript received 21 Oct 2024; accepted for publication 25 Oct 2024; published online 16 Nov 2024. doi: 10.18287/JBPE24.10.040308.

1 Introduction

Cell viability analysis has attracted much attention as a substitute for animal testing. This is necessary, for example, when screening large numbers of chemicals for their cytotoxicity on various cell types.The traditional quantitative cell viability test involves the addition of exogenous agents such as 3-(4,5-dimethyl-2-thiazolyl)-2,5-diphenyl-2H-tetrazolium bromide (MTT), which has been one of the most commonly used dyes for colorimetric assessment of cell viability since the early 1980s [1]. This assay is now presented as a rapid, accurate, and simple method for the detection of live cells in mammalian cell cultures.

MTT is a yellow water-soluble tetrazolium salt [2] that is converted into a water-insoluble formazan [3, 4] by reductive cleavage of the tetrazolium ring by mitochondrial dehydrogenases in living cells. Since dead cells are unable to produce dehydrogenase during metabolic processes, they do not possess this reductive capacity.

The key steps of the traditional MTT assay include incubation of cells with MTT, removal of the cell culture medium containing formazan crystals from the cells, solubilization of formazan, and measurement of the optical density to determine the amount of formazan using a microplate spectrophotometer [4]. Thus, the assay results depend on the ability of metabolically active cells to reduce MTT to formazan. In other words, the amount of formazan detected spectrophotometrically serves as an indicator of the number of mitochondria, which, in turn, corresponds to the number of living cells in the sample [5, 6].

The MTT assay has been shown to be useful for monitoring cell viability independent of proliferative

activity [1], and for quantifying mitochondrial activity [7]. In addition, MTT assays have been used to study chemosensitivity, radiosensitivity, and toxicity of drugs in human tumor cell lines [8]. Cytotoxic effects of drugs on the development of various forms of cancer have also been reported using the MTT assay [9, 10].

As noted, the conventional MTT method is a robust quantitative method with distinct advantages, such as being time- and cost-effective, and the use of microplate scanning spectrophotometers allows for the processing of large numbers of samples. Nevertheless, it has certain limitations, including significant interference from other substances and a low detection sensitivity (approximately 1.0 μg/mL), as well as the tendency to produce false positive results [11]. The addition of organic solvents to serum-containing medium results in the precipitation of serum proteins, which affects absorbance measurements [12]. In addition, a 4 h incubation period is typically required, which may be extended for low-density cells or cells with a lower metabolic rate, prior to spectrophotometric assessment of their viability [8]. A small amount of formazan can be lost during the removal of the culture medium, which can bias the experimental results. These observations have led to the search for various alternative assays [13]. Increasing the detection sensitivity of MTT assays and simplifying the steps remains an important challenge. Moreover, the precise nature of the interactions between MTT salts and living cells at very low concentrations (ng/mL) in situ needs to be elucidated. To obtain information at such dilute levels, non-destructive assay approaches are needed that combine sensitivity, chemistry, and spatial resolution.

Here we propose a combination of MTT analysis with surface-enhanced Raman spectroscopy (SERS), which can fulfill all of these requirements. SERS combines the advantages of in situ molecular identification [14], offline detection, well-established instrumentation, exceptional sensitivity, non-invasiveness and virtually no sample preparation [15−19]. Advances in both laser and detector technologies, as well as an improved understanding of the SERS mechanism, have led to the application of SERS for single-molecule detection [20]. Beyond this fundamental limit in chemical analysis, SERS has also been employed in various biological applications, such as the identification and classification of viruses or cancer cells [21, 22], as well as in biochemical diagnostics [23, 24], pH sensing [25], and pharmaceutical research [26]. The characteristic Raman bands of biological macromolecules can be used to track the changes of various components before and after apoptosis using Raman imaging. The introduction of the SERS probe into the cell not only increases the sensitivity of Raman imaging, but also enables dynamic observation of intracellular organelle interactions, providing a more convenient and intuitive detection method.

In our work, a novel type of SERS platform, consisting of silica microspheres coated with gold nanostars, was developed and combined with Raman imaging technology and traditional MTT assay to determine the viability of single cells *in situ*. This overcomes the limitations of the traditional MTT method in terms of complex sample pretreatment steps and provides a new method to assess cell apoptosis in situ in real time. Furthermore, Raman spectroscopy-based cell imaging methods have emerged as powerful tools in cell biology because the molecular composition of subcellular compartments can be visualized without the additional labeling [27] and within a relatively short time frame (typically minutes) compared to traditional methods that are typically time-consuming. Thus, the proposed method has great potential for use in highly sensitive and highly efficient cell imaging methods.

2 Materials and Methods

2.1 Formazan Synthesis

To reduce MTT to formazan we added glucose in a 10-fold excess to an aqueous solution of MTT with a concentration of 1 mg/mL and pH = 10. After 2 h, the resulting formazan suspension was washed with water and dried for 2 days at 40 °C.

2.2 Gold Nanostars Synthesis

Gold nanostars were synthesized using a two-step protocol using gold seed particles [28, 29], with minor modifications. In the first step, gold nanospheres with an average diameter of 15 nm were synthesized using the Frens method [30], and used as seeds for the synthesis of gold nanostars. For this, 238 mL of water were boiled in an Erlenmeyer flask while stirring on a magnetic stirrer. 2.5 mL of 1% $HAuCl_4$ solution and 7.75 mL of 1% sodium citrate solution were added. The solution was stirred for 15 min, during which time the color of the solution changed from colorless to red. In the second step, to synthesize nanostars, 46.25 mL of water, 3.75 mL of 10 mM $HAuCl_4$ and 150 μL of 1 M HCl were successively added to 4.5 mL of 15-nm seed particles with a concentration of $1.6 \cdot 10^{12}$ mL^{-1}. Then, 750 μL of 4 mM silver nitrate and 750 μL of ascorbic acid (AA; 100 mM) were added with stirring (700 rpm). The solution was stirred for 30 s, during which its color quickly changed from light red to blue-green. Then, 5 mL of 1% polyvinylpyrrolidone (PVP) solution (10 kDa) in ethanol was added to the colloid with stirring and stirred for additional 10 min. Then, gold nanostars were purified from reaction products by centrifugation (5000 rpm, 10 min) and resuspended in 20 mL of ethanol.

2.3 Concentration vs SERS and Absorbance Calibration Plots

To plot the calibration dependence, a series of successively diluted formazan solutions in a 1:1 mixture of water and isopropyl alcohol were prepared. The calibration dependence of absorption on the concentration of formazan was made by measuring absorption at a wavelength of 560 nm for different concentrations of the reactant. SERS calibration dependence was made as follows. The gold nanostars colloid (100 μL) with an optical density of 1.4 (measured

in 1 cm cuvette) was added to 900 mL of the formazan solutions with different concentrations and the Raman spectra of the resulting mixture were recorded. A PeakSeeker Pro setup (Ocean optics, USA) was used to measure the Raman spectra. The measurements were carried out in 1 cm four-sided quartz cuvettes with excitation at a wavelength of 785 nm. The laser radiation power was 30 mW, the signal accumulation time was 10 s. To reduce the effect of the internal filter, the laser beam was focused near the wall of the cuvette.

2.4 SERS Platform Preparation

To synthesize isodisperse silica microparticles, we used a multistage overgrowth method, described in detail in our work [31]. The number of overgrowth cycles was selected so that the size of the silica particles was about 2 μm.

For the adsorption of gold nanostars, the surface of silica microparticles was functionalized with amino groups by doping with aminopropyltrimethoxysilane. The corresponding silane was added to a colloid of 2 μm silica particles in ethanol in an amount of 1% of the reaction mixture volume. The particle suspension was incubated for 1 h at room temperature with stirring. The resulting aminated particles were centrifuged at 5000 rpm for 1 min and resuspended in ethanol again using ultrasonic treatment.

Next, 1 mL of the colloid of functionalized silica particles was added to 4 mL of concentrated colloid of gold nanostars (Optical density, OD = 20). The resulting mixture was incubated for 24 h with stirring at 500 rpm. The particles were then centrifuged at 5000 rpm for 1 min and resuspended in ethanol.

The extinction spectra were recorded using a Specord S300 spectrophotometer (Analytik Jena, Germany). The measurements were performed in the wavelength range of 320−1100 nm using quartz cuvettes with an optical path length of 2 mm and 10 mm.

The size and electrokinetic potential of gold nanoparticles and silica particles were measured using a Zetasizer ZS setup (Malvern, UK).

Transmission electron microscopy (TEM) images were obtained using a Libra-120 transmission electron microscope (Carl Zeiss, Germany) at the Simbioz Center for the Collective Use of Research Equipment in the Field of Physical Chemical Biology and Nanobiotechnology, IBPPM RAS, Saratov.

Scanning electron microscopic images were obtained using a Mira-II LMU microscope (Tescan, Czech Republic). For analysis, samples of nano- and microparticles were applied to a silicon substrate, the accelerating voltage during the study was 30 kV.

The concentration of silica microparticles was determined gravimetrically by weighing the dry residue after lyophilization of the colloid on an analytical balance. The total weight of particles in 1 mL of the colloid allow us to unambiguously determine the numerical concentration of particles using the following Eq.:

$$N = \frac{3m}{4\rho r R^3},$$

where m is the mass of silica, expressed in mg, ρ is the density of silica, expressed in mg/cm^3, R is the radius of the particles, expressed in centimeters. The mass of the silicate particle with a diameter of 2 μm is the product of the density by the volume of the particle and is $7.12 \cdot 10^{-9}$ mg. The suspension has a concentration of silicate particles of 20 mg/mL or $2.86 \cdot 10^9$ mL^{-1}.

2.5 Metabolic Cells Activity Test

Undifferentiated murine colon carcinoma cell line (CT26.WT) was used in experiments on cytotoxicity, internalization and detection of formazan inside cells. CT26.WT was cultured in Dulbecco's Modified Eagle Medium (DMEM) supplemented with a 10% Fetal bovine serum (FBS), and 1% penicillin / streptomycin.

The relative metabolic activity of CT26.WT cells after incubation with SERS platforms was measured using MTT reagent. Cells were seeded in 96-well plates at a density of 5×10^3 cells per well and left in humidify atmosphere containing 5% CO_2 at 37 °C. The next day, the SERS platforms were added to the wells at predefined concentration (1, 2, 3, 4, 5, 10, 15, 20, 25, 30, and 50 SERS platforms per cell) with fresh media after aspiration of the old media. For control cells group, only medium replacement was performed. Further cell incubation was carried out at 37 °C and in an atmosphere containing 5% CO_2. After 48 h, the media was aspirated and replaced with 90 μL of the fresh media, followed by the addition of MTT reagent (10 μL) dissolved in PBS (5 mg/mL). The culture media from well (75 μL) of were aspirate and 75 μL of Dimethyl sulfoxide (DMSO) were added after 4 h of cells incubation with MTT reagent. The final solution with DMSO in the wells was carefully pipetting, and plate was left at 37 °C for 10 min. Optical density (OD) of formazan solution in the wells was measured at wavelength of 554 nm using CLARIOstar Plus Microplate Reader (BMG Labtech, Germany). Relative metabolic activity was calculated as the ratio of the OD mean value in the wells where cells were incubated with SERS platforms to the OD mean value of the control group, expressed as a percentage.

2.6 Microscopy Study of Particles Internalization

CT26.WT cells were seeded in SPL Confocal Dishes (SPL Life Sciences Co., Ltd.) at a density 300×10^3 cells and left in humidify atmosphere containing 5% CO_2 at 37 °C. The next day, the SERS platforms were added to the Confocal Dishes at concentration of 30 SERS platforms per cell with fresh media after aspiration of the old media. Incubation lasted 48 h at 37 °C and in an atmosphere containing 5% CO_2. After the co-incubation period, the cells were washed with Ca- and Mg-free Dulbecco's Phosphate-Buffered Saline (DPBS), fixed with 2.5% glutaraldehyde for 8 h, and prepared for scanning electron and atomic force microscopy. For this purpose, dehydration was performed by sequential soaking in ethanol/water solutions with increasing alcohol concentrations (50%, 60%, 70%, 80%, 90%, and

99.9%) for 30 min. Drying of the cell layer at the bottom of the Confocal Dishes was accomplished with Hexamethyldisilizane (HMDS). The 99.9% ethanol in the Confocal Dishes was replaced with a 1:2 solution of HMDS: 99.9% ethanol, then with a 2:1 solution of HMDS: 99.9% ethanol, and finally with 100% HMDS. The exposure to solutions containing HMDS lasted 20 min. Cells' layer was exposed to 100% HMDS twice and then left for drying in the fume hood overnight.

To study the morphology and microstructure, dried cell layer with particles were sputtered with gold and imaged with scanning electron microscopes MIRA II LMU at an operating voltage of 15 kV.

Atomic force microscopy (AFM) measurements were performed in tapping mode on an NTEGRA spectra setup (NT-MDT-SI, Zelenograd, Russia) using NSG10 probes. Alignment and artifact correction were performed using Gwiddion 2.6 software.

2.7 Cell Preparation for Raman Spectroscopy

For cell preparation for Raman spectroscopy quartz glasses (15 × 15 mm) were coated with poly-D-lysine (100 μg/mL) preliminary. CT26.WT cells were seeded in Petri Dishes 35 mm (Nunc™ Cell Culture/Petri Dishes, Thermo Scientific) with quartz glass located at the bottom at a density 300×10^3 cells and left in humidify atmosphere containing 5% CO_2 at 37 °C. The next day, the particles were added to the Petri Dishes at concentration of 30 particles per cell with fresh media after aspiration of the old media. Incubation lasted 48 h at 37 °C and in an atmosphere containing 5% CO_2. After the co-incubation period, the cells were washed with Ca- and Mg-free DPBS and MTT solution in complete culture media was added (1 mL). MTT solution consisted of complete culture (90% v/v) and Stock MTT solution in DPBS at concentration 5 mg/mL (10% v/v). The biochemical reaction was stopped by aspirating the MTT solution and washing the cell layer with DPBS without Ca and Mg. For Raman Spectroscopy, 5 mL of DPBS without Ca and Mg was added to the Petri dish. Measurements were taken 20 and 60 min after adding the MTT solution to the cells.

Raman spectra were collected using a Renishaw InVia Raman spectrometer (Renishaw, UK), equipped with a 785 nm laser. Drops of SiO_2 microparticles from the suspension and formazan solution (0.1 mg/mL) in ethanol were deposited onto a quartz substrate. A Raman map of the air-dried mixture was obtained with a 50×/0.5 NA objective (Leica, Germany), using 0.1% (25 μW) laser power and 1 second per single spectrum acquisition time. Raman maps of cells on a quartz substrate were also collected with a Leica 63×/0.9 NA water-immersion objective, using 1% (250 μW) laser power, and 1 s/spectrum acquisition time.

All collected spectra were processed using Renishaw WiRE software version 4.2, which removed cosmic rays and a polynomial baseline fit of order 11. The data were then analyzed using Python 3 in the Jupyter notebook environment. Mean spectra were calculated from data with intensities above 95% percentile for microparticles or 75% percentile for cells.

3 Results

In the first stage of the study we decided to compare the possibility of detecting formazan in solution using spectrophotometry and SERS. It is important to note that a laser with a wavelength of 785 nm is used for SERS experiments, which is most widely used for SERS mapping of biological objects due to the significant penetration depth of near-IR radiation into biological tissues and low autofluorescence of biological tissues [32]. It was previously reported that MTT-formazan has a very low Raman scattering cross-section when irradiated with a 785 nm laser [15].

MTT is a yellow water-soluble tetrazolium salt. MTT is reduced in the mitochondria of metabolically active cells by succinate dehydrogenase to yield a water-insoluble purple formazan crystal [33, 34], which can be spectrophotometrically measured upon solubilization. Outside cells, formazan is formed from MTT by reduction (Fig. 1) with plant extracts [35], tocopherols [36], and flavonoids [37].

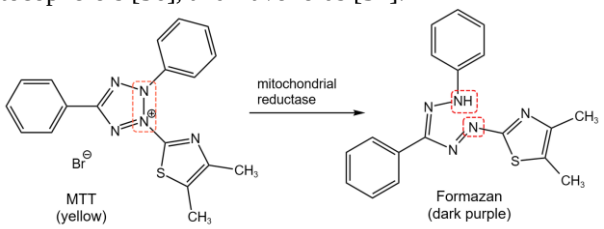

Fig. 1 Scheme of the cleavage proceeding of the MTT salt to formazan. The red dotted line indicates the N-N bond, through which reduction occurs with the opening of the heterocycle.

To reduce MTT to formazan, glucose was used in a 10-fold excess compared to an aqueous solution of MTT with a concentration of 1 mg/mL and pH = 10 (pH was adjusted by the addition of 1 M sodium hydroxide). After 2 h, the resulting formazan suspension was washed with water and dried for 2 days at 40 °C.

Gold nanostars were used as amplifiers of the SERS signal. To obtain gold nanostars, a seed particle protocol was implemented [38, 39], where 15-nm quasi-spherical gold particles were used as nanostars growth centers. In our case, gold was reduced on the seed surface using ascorbic acid, and silver chloride obtained directly in the colloid by reacting silver nitrate with hydrochloric acid was used to create anisotropic growth conditions. By varying the concentration of gold seeds and the amount of gold-containing precursor, it is possible to regulate the size of the stars and the number of "tips" [38, 40].

The synthesized nanoparticles were characterized by transmission electron microscopy. Thus, from the transmission electron microscopy data (Fig. 2a) it is evident that the average size of the core of such particles was about 40 nm, the length of the rays was 15−20 nm and the number of "tips" was from 3 to 10. The data on the size parameters of the nanostars obtained from TEM micrographs are in good agreement with the values determined by the dynamic light scattering (measured in ethanol), which were 68.8 ± 26.2 nm.

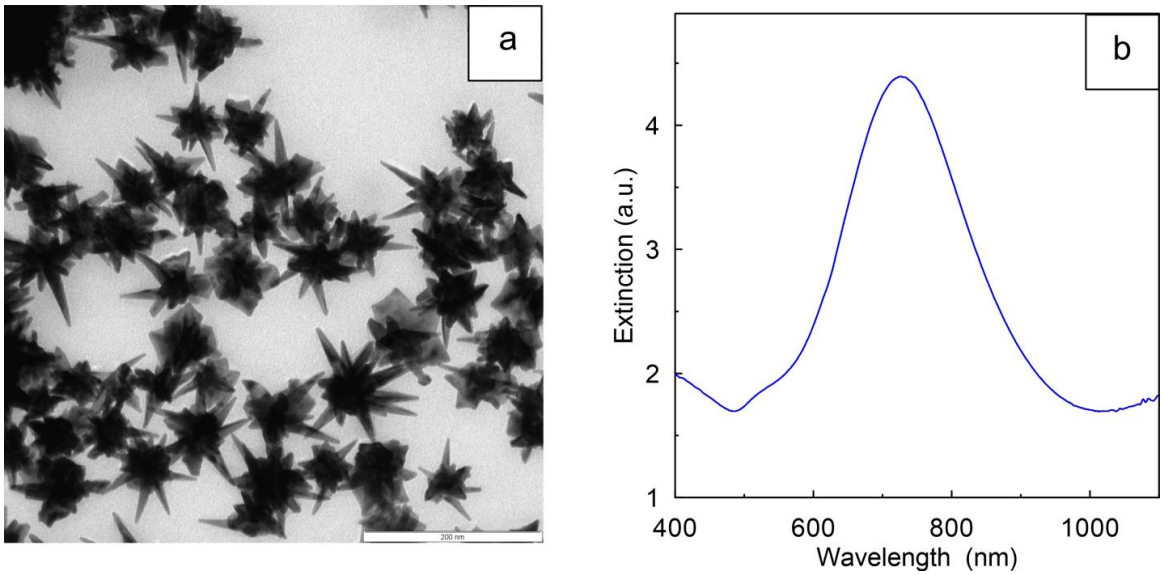

Fig. 2 (a) Electron microscopy images of gold nanostars obtained by reducing the gold-containing precursor with ascorbic acid on the surface of 15-nm "seeds". The scale bar is 200 nm. (b) The extinction spectrum of the synthesized nanoparticles.

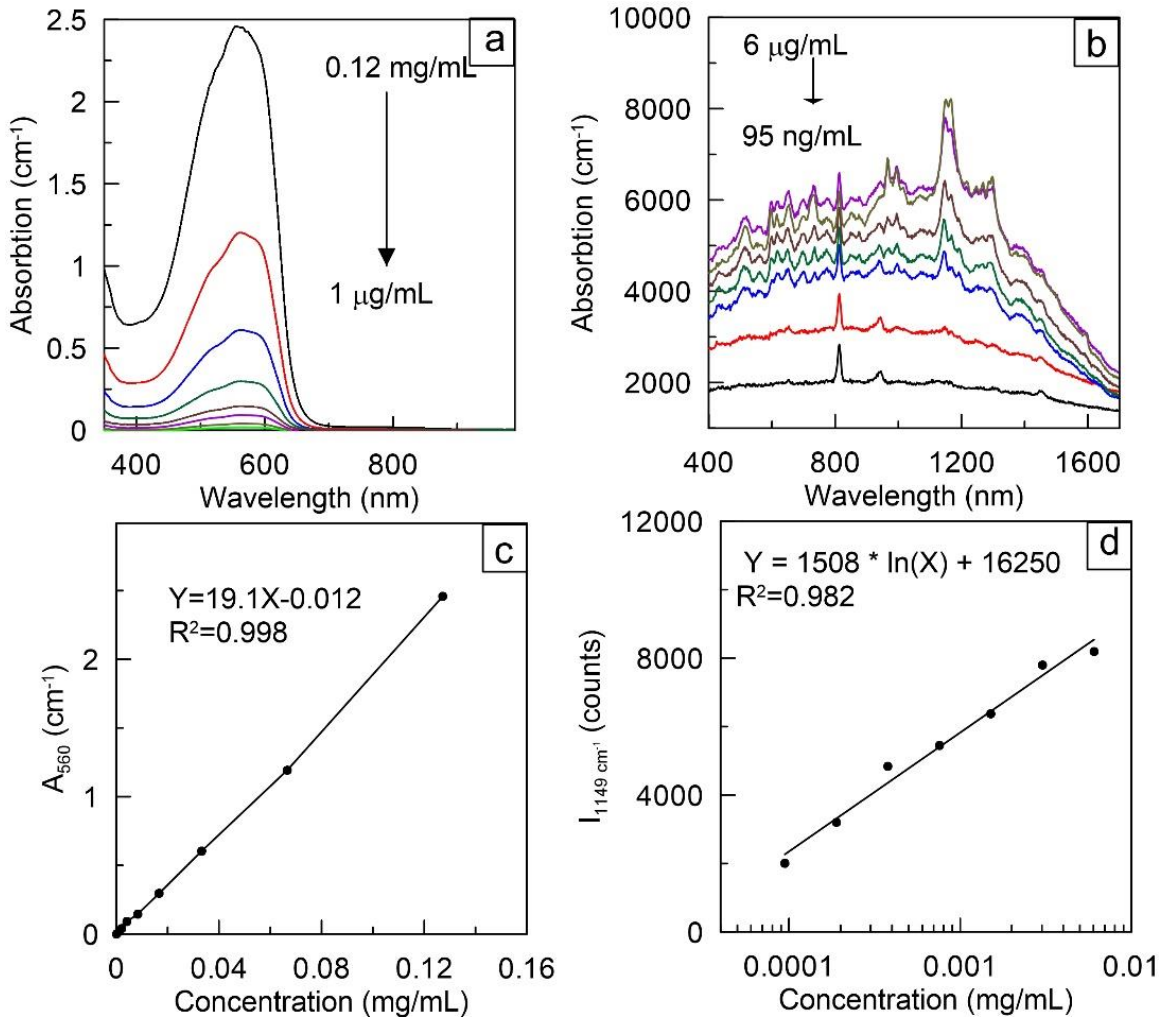

Fig. 3 (a) Absorption spectra of MTT-formazan solutions in isopropyl alcohol with concentrations of 120^{-1} μg/mL. (b) SERS spectra of MTT-formazan on gold nanostars in a colloid. The formazan concentration is 6 μg–95 ng/mL. Calibration curves for determining the formazan concentration in solution by (c) absorption at a wavelength of 560 nm and (d) SERS intensity at 1176 cm^{-1}.

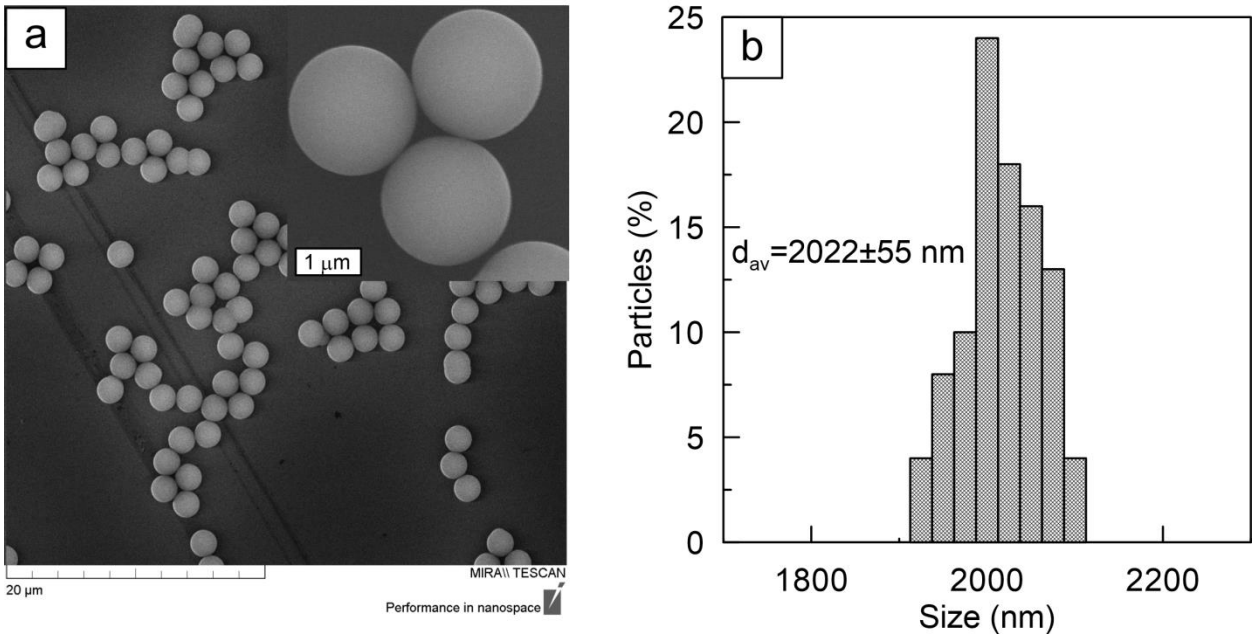

Fig. 4 (a) Scanning electron microscopic image of silicate microparticles. Scale bar is 20 μm. The inset shows an enlarged image of individual particles. Scale bar is 1 μm. (b) Histogram of the size distribution of silicate particles.

Fig. 2b shows the extinction spectra of the gold nanostars colloid. In agreement with our previous studies [41], there is maximum in the extinction spectrum at 720 nm. Also the extinction spectrum has a shoulder in NIR region. These spectral features are typical for nanostars with rough core and thin and sharp tips.

In general, it can be expected that the measured optical properties of the nanoparticles will allow obtaining an enhanced electromagnetic field near the rays when excited by laser radiation in the red and near infrared range.

Fig. 3a shows the absorption spectra of MTT-formazan at concentrations up to 120 μg/mL. It is evident that there is a well-known absorption maximum at 560 nm. The calibration curve in Fig. 3c shows excellent linearity ($R^2 = 0.998$) of the dependence of the formazan absorption intensity on its concentration in solution. The detection limit using a 1 cm cuvette was aproximately 1 μg/mL.

To determine the possibility of detecting formazan by SERS, 1 mL of an aqueous colloid of gold nanostars with an OD of 1.4 (measured in 1 cm cuvette) was mixed with 100 μL of a formazan solution in isopropanol (final concentration of 6 μg − 95 ng/mL). Then, the SERS spectrum of the resulting colloid was measured in a four-sided quartz cuvette.

Fig. 3b shows the measured SERS spectra. A decrease in the SERS intensity with a decrease in the formazan concentration is evident. It should be noted that the spectral lines at 819, 953, and 1454 cm^{-1} are related to isopropanol and have a constant intensity, since its concentration in all samples is the same. These spectral lines can be used as an internal standard, if necessary, to check the same laser focusing for all samples.

To construct a calibration dependence for determining the concentration of MTT-formazan by SERS, the most intense peak of formazan at 1176 cm^{-1} was used. The resulting calibration dependence is shown in Fig. 3d. It should be noted that, unlike the spectrophotometric dependence, it has a semi-logarithmic rather than linear form, which is typical for all SERS calibrations. It worth mentioning that the minimum detection limit of formazan by SERS was almost an order of magnitude lower than using spectrophotometry while maintaining a high correlation coefficient. Thus, formazan can be effectively detected by analyzing the SERS signal excited at 785 nm.

Isodispersed SiO_2 particles were used as a matrix for assembling gold nanostars in SERS active microstructures. Fig. 4a shows scanning electron microscopic images of such particles.

The inset on Fig. 4a shows an enlarged image demonstrating the ideal spherical shape of the SiO_2 particle. Fig. 4b shows a histogram of the size distribution of silicate microparticles, the average diameter 2022 ± 55 nm. For the subsequent adsorption of gold nanostars, silicate microparticles were functionalized with aminopropyltrimethoxysilane to introduce amino groups with a positive charge. The initial silicate microparticles in water had an electrokinetic potential of −33.2 ± 4.6 mV. After the amination procedure, the electrokinetic potential was +13.8 ± 6.2 mV.

In contrast to the commonly used SERS platforms based on individual spherical gold or silver nanoparticles [42−44], in this work, PVP-stabilized gold nanostars were assembled via electrostatic interactions on the surface of positively charged amino-functionalized silica microspheres. The insets in Fig. 5a show scanning electron microscopy (SEM) images of silica microspheres with surface-adsorbed gold nanostars.

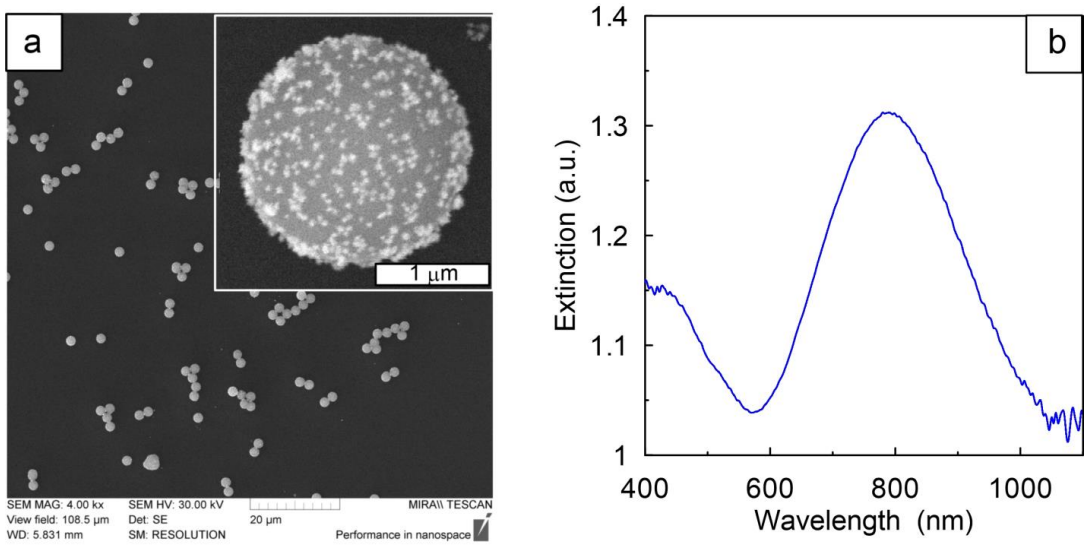

Fig. 5 Panel (a) shows the electron microscopic image of silica microspheres with surface-adsorbed gold nanostars. Scale bars are 20 μm and 1 μm in the insert. Panel (b) shows the extinction spectrum of the synthesized SERS platforms.

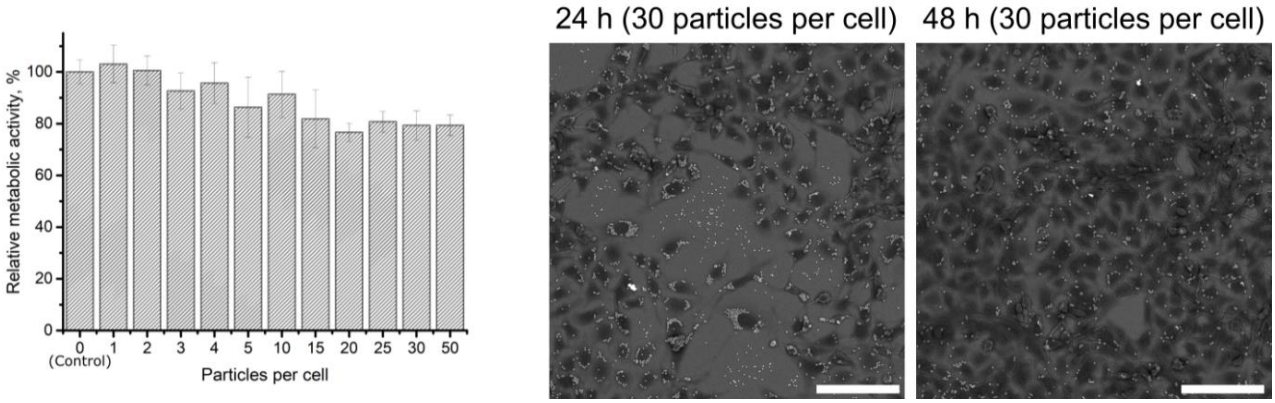

(a) (b) (c)

Fig. 6 Study of particles' impact on mouse colorectal carcinoma cells (CT26.WT) during 48 h of co-incubation. (a) Relative metabolic activity of CT26.WT after 48 h of incubation with particles added at different concentrations. Scanning electron microscopy (SEM) images of CT26.WT after (b) 24 h and (c) 48 h of incubation. SEM images obtained in backscattered electron (BSE) mode. Scale bar corresponds to 100 μm.

It is important to note that the silica microparticles after adsorption of gold nanostars retained colloidal stability, were not aggregated, and in the SEM image (Fig. 5a) the microspheres are separated from each other. The extinction spectra SiO_2@AuNst shown in the Fig. 5b demonstrate that the positions of the surface plasmon resonance peaks for stars adsorbed on silica microspheres differ from those for the original colloid. In this case, the plasmon resonance peak broadens and shifts to the near IR region of the spectrum.

The effect of the designed particles on cellular metabolic activity and determination of particle concentrations that exert significant cytotoxic effect were studied on mouse colorectal carcinoma cells (CT26.WT). The study was conducted in a wide range of added particles (Fig. 6a).

The most pronounce decrease in metabolic activity was observed with the addition of 15 or more particles per cell. However, such a decrease did not exceed 24% even for the case of co-incubation of cells and particles at a concentration of 50 particles per cell. Study of cell morphology during co-incubation with particles (30 particles per cell) after 24 and 48 h by scanning electron microscopy did not reveal areas of dead cells (Fig. 6 b, c). After the specified time, the cells had normal morphology (as they were elongated and adhered to the bottom), and their number also increased significantly between 24 and 48 h. Thus, it can be concluded that the developed SERS platform does not have any toxic effects *in vitro*.

In the images obtained by scanning electron and atomic force microscopy spread cells with pseudopodia can be seen (Fig. 7a, b). The constructed surface profiles of the obtained AFM images (Fig. 7c) allow us to distinguish particles adhered to the cell membrane on the cell surface (profile 1) from particles internalized by the cell (profile 2).

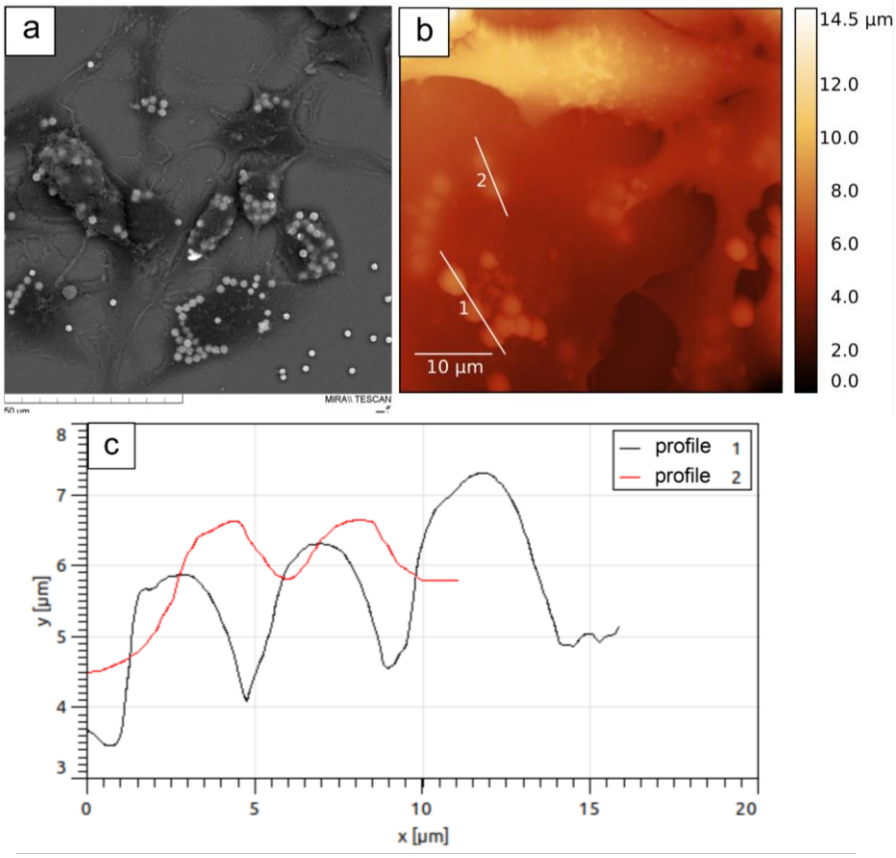

Fig. 7 Particle internalization by CT26.WT cells. (a) Scanning electron microscopy in backscattered electron (BSE) detection mode. Scale bar is 50 µm. (b) AFM of a cell layer after 48 h of incubation with SERS platforms. (c) Surface profile of AFM image.

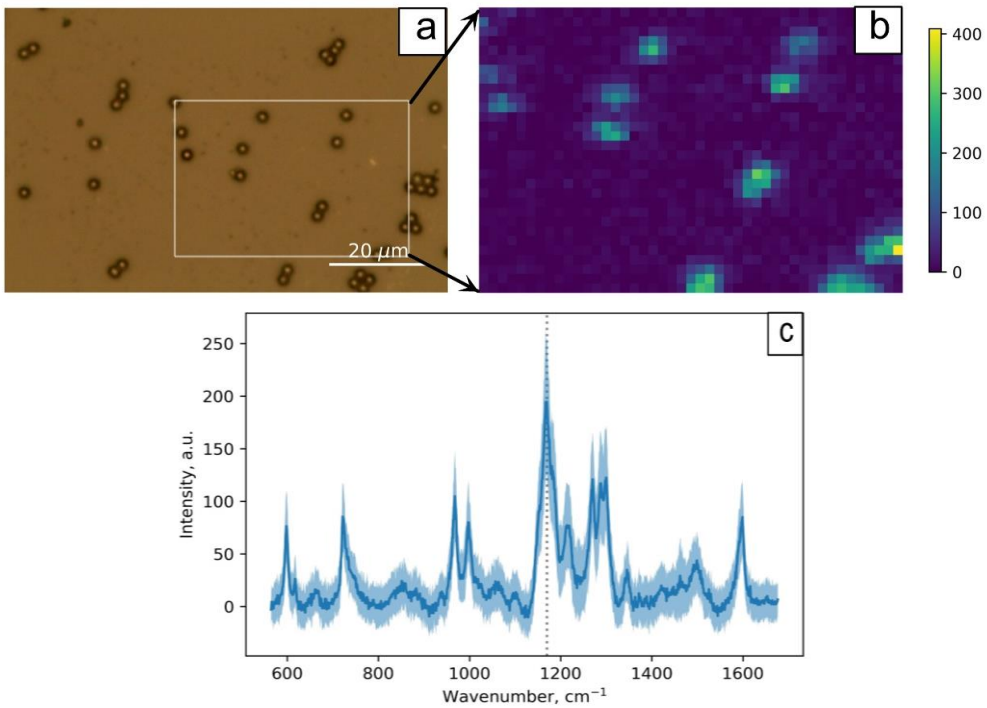

Fig. 8 (a) Microscopic image of SiO_2@AuNst microparticles deposited on quartz glass together with formazan. (b) SERS map of SiO_2@AuNst microparticles deposited on quartz glass together with formazan. (c) Averaged SERS spectrum of different SiO_2@AuNst microparticles and spectrum variations from particle to particle. The image is decoded by the intensity of the characteristic line. Panel (c) shows mean SERS spectrum with standard deviation of the studied microparticles.

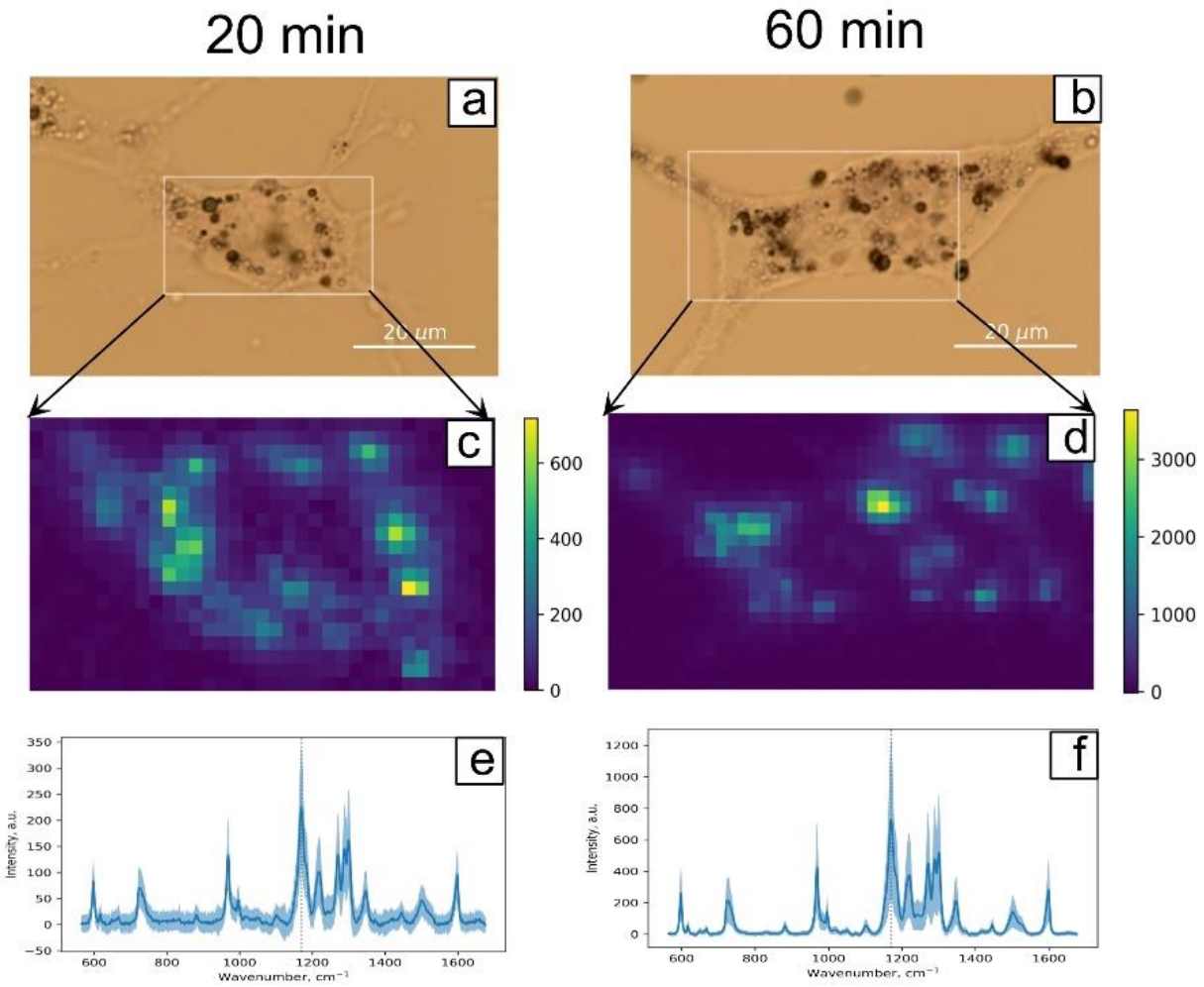

Fig. 9 Microscopic images of CT26.WT cells incubated with SiO_2@AuNst microparticles at a concentration of 30 pieces per cell (a) 20 and (b) 60 min after the addition of formazan. (c, d) SERS mapping of these cells. (e, f) SERS spectra (mean and standard deviation) of formazan inside the cells measured using SiO_2@AuNst microparticles.

Our main goal was to demonstrate the possibility of local detection of formazan using the developed SiO_2@AuNst microplatform. To test the assumption of the possibility of local detection, the platforms were mixed with a formazan solution (0.1 mg/mL) and dried on the surface of quartz glass. Then, SERS mapping of the area containing microparticles and their aggregates was performed, and the signal levels on the microparticles and in the areas where there was only formazan without particles were estimated. Fig. 8a shows a microscopic image of microparticles dried from a mixture with formazan. Due to the 2 μm size, the particles are easily visualized using a conventional optical microscope with a 40× objective. The mapping area is marked with a white rectangle. Mapping was performed with a resolution of 1 μm. The SERS image constructed from the intensity of the most pronounced line at 1176 cm^{-1} (Fig. 8b) shows that the position and number of particles coincide with the optical image, and outside the particles, the signal from formazan is at the noise level. The averaged spectra from different particles and the signal variation are shown in Fig. 8c. The signal level variation within 20% from particle to particle is visible.

To test the possibility of detecting formazan inside cells using the developed SERS platforms, cells were incubated with microparticles and individual living cells were mapped 20 and 60 min after adding MTT.

Fig. 9 a, b shows microscopic images of cells after incubation with microparticles and adding MTT. Microparticles accumulated inside the cells are visible in the optical image. To assess the enzymatic activity, SERS mapping of the cell was performed (Fig. 9c, d). In both cases, formazan accumulation in the cells was observed, and it was especially easily detected in the area of localization of the SERS microplatforms. It should be noted that the absolute signal level after 60 min was 4 times higher than after 20 min (Fig. 9e, f). However, even after 20 min, it is quite detectable. Thus, the developed platforms and SERS detection technique allows one to study enzymatic activity at the level of a single cell based on the level and distribution of the SERS signal from MTT-formazan. An additional advantage is the ability to evaluate these parameters within 20 min

after adding the reagent and the absence of the need to dissolve formazan with dimethyl sulfoxide.

4 Conclusions

A novel type of SERS platform, consisting of silica microspheres coated with gold nanostars, was developed and combined with Raman imaging technology and traditional MTT assay to determine the viability of single cells *in situ*. First, the formazan concentration can be determined from the SERS signal intensity without performing the extraction and enrichment steps. Second, the SERS spectra of formazan can be directly obtained at the level of a single particle internalized by the cell. Based on the characteristics of SERS, the SERS-MTT detection method is expected to avoid interference from background substances (such as residual MTT reagent, serum, exogenous drugs) in cell suspensions. In addition, the proposed approach not only simplifies the testing procedure, but we also expect it to have a higher accuracy in assessing the efficacy of anticancer drugs compared to the traditional MTT method.

Acknowledgment

The study was supported by Russian Science Foundation, grant No. 23-24-00062.

Disclosures

The authors declare that they have no conflict of interest.

References

1. T. Mosmann, "Rapid colorimetric assay for cellular growth and survival: Application to proliferation and cytotoxicity assays," Journal of Immunological Methods 65(1–2), 55–63 (1983).
2. A. M. Mattson, C. O. Jensen, and R. A. Dutcher, "Triphenyltetrazolium chloride as a dye for vital tissues," Science 106(2752), 294–295 (1947).
3. A. S. Shawali, N. A. Samy, "Functionalized formazans: A review on recent progress in their pharmacological activities," Journal of Advanced Research 6(3), 241–254 (2015).
4. F. M. Young, W. Phungtamdet, and B. J. S. Sanderson, "Modification of MTT assay conditions to examine the cytotoxic effects of amitraz on the human lymphoblastoid cell line, WIL2NS," Toxicology in Vitro 19(8), 1051–1059 (2005).
5. F. Denizot, R. Lang, "Rapid colorimetric assay for cell growth and survival," Journal of Immunological Methods 89(2), 271–277 (1986).
6. T. J. M. Patricia Price, Trevor J. McMillan, "Use of the tetrazolium assay in measuring the response of human tumor cells to ionizing radiation," Cancer Research 50(5), 1392–1396 (1990).
7. D. Gerlier, N. Thomasset, "Use of MTT colorimetric assay to measure cell activation," Journal of Immunological Methods 94(1−2), 57−63 (1986).
8. K. Buch, T. Peters, T. Nawroth, M. Sänger, H. Schmidberger, and P. Langguth, "Determination of cell survival after irradiation via clonogenic assay versus multiple MTT Assay - A comparative study," Radiation Oncology 7(1), 1 (2012).
9. E. Ulukaya, F. Ozdikicioglu, A. Y. Oral, and M. Demirci, "The MTT assay yields a relatively lower result of growth inhibition than the ATP assay depending on the chemotherapeutic drugs tested," Toxicology in Vitro 22(1), 232–239 (2008).
10. Z. Chen, G. Liu, M. Chen, B. Xu, Y. Peng, M. Chen, and M. Wu, "Screen anticancer drug in vitro using resonance light scattering technique," Talanta 77(4), 1365–1369 (2009).
11. N. T. H. Nga, T. T. B. Ngoc, N. T. M. Trinh, T. L. Thuoc, and D. T. P. Thao, "Optimization and application of MTT assay in determining density of suspension cells," Analytical Biochemistry 610, 113937 (2020).
12. R. Foldbjerg, D. A. Dang, and H. Autrup, "Cytotoxicity and genotoxicity of silver nanoparticles in the human lung cancer cell line, A549," Archives of Toxicology 85(7), 743–750 (2011).
13. P. Marqués-Gallego, H. den Dulk, C. Backendorf, J. Brouwer, J. Reedijk, and J. F. Burke, "Accurate non-invasive image-based cytotoxicity assays for cultured cells," BMC Biotechnology 10(1), 43 (2010).
14. 14. J. Kneipp, H. Kneipp, and K. Kneipp, "SERS—a single-molecule and nanoscale tool for bioanalytics," Chemical Society Reviews 37(5), 1052 (2008).
15. Z. Mao, Z. Liu, L. Chen, J. Yang, B. Zhao, Y. M. Jung, X. Wang, and C. Zhao, "Predictive value of the surface-enhanced resonance raman scattering-based mtt assay: a rapid and ultrasensitive method for cell viability in situ," Analytical Chemistry 85(15), 7361–7368 (2013).
16. B. Zhang, H. Wang, L. Lu, K. Ai, G. Zhang, and X. Cheng, "Large-area silver-coated silicon nanowire arrays for molecular sensing using surface-enhanced raman spectroscopy," Advanced Functional Materials 18(16), 2348–2355 (2008).
17. A. Musumeci, D. Gosztola, T. Schiller, N. M. Dimitrijevic, V. Mujica, D. Martin, and T. Rajh, "SERS of semiconducting nanoparticles (TiO 2 hybrid composites)," Journal of the American Chemical Society 131(17), 6040–6041 (2009).

18. S. Lee, S. Kim, J. Choo, S. Y. Shin, Y. H. Lee, H. Y. Choi, S. Ha, K. Kang, and C. H. Oh, "Biological imaging of hek293 cells expressing plcγ1 using surface-enhanced raman microscopy," Analytical Chemistry 79(3), 916–922 (2007).
19. J. R. Lombardi, R. L. Birke, "A unified view of surface-enhanced raman scattering," Accounts of Chemical Research 42(6), 734–742 (2009).
20. B. Tolaieb, C. J. L. Constantino, and R. F. Aroca, "Surface-enhanced resonance Raman scattering as an analytical tool for single molecule detection," Analyst 129(4), 337 (2004).
21. S. Shanmukh, L. Jones, Y.-P. Zhao, J. D. Driskell, R. A. Tripp, and R. A. Dluhy, "Identification and classification of respiratory syncytial virus (RSV) strains by surface enhanced Raman spectroscopy and multivariate statistical techniques," Analytical and Bioanalytical Chemistry 390(6), 1551–1555 (2008).
22. X. Qian, X.-H. Peng, D. O. Ansari, Q. Yin-Goen, G. Z. Chen, D. M. Shin, L. Yang, A. N. Young, M. D. Wang, and S. Nie, "In vivo tumor targeting and spectroscopic detection with surface-enhanced Raman nanoparticle tags," Nature Biotechnology 26(1), 83–90 (2008).
23. J.-H. Kim, J.-S. Kim, H. Choi, S.-M. Lee, B.-H. Jun, K.-N. Yu, E. Kuk, Y.-K. Kim, D. H. Jeong, M.-H. Cho, and Y.-S. Lee, "Nanoparticle probes with surface enhanced raman spectroscopic tags for cellular cancer targeting," Analytical Chemistry 78(19), 6967–6973 (2006).
24. K. Hering, D. Cialla, K. Ackermann, T. Dörfer, R. Möller, H. Schneidewind, R. Mattheis, W. Fritzsche, P. Rösch, and J. Popp, "SERS: a versatile tool in chemical and biochemical diagnostics," Analytical and Bioanalytical Chemistry 390(1), 113–124 (2008).
25. Z. Wang, A. Bonoiu, M. Samoc, Y. Cui, and P. N. Prasad, "Biological pH sensing based on surface enhanced Raman scattering through a 2-aminothiophenol-silver probe," Biosensors and Bioelectronics 23(6), 886–891 (2008).
26. R. Stevenson, R. J. Stokes, D. MacMillan, D. Armstrong, K. Faulds, R. Wadsworth, S. Kunuthur, C. J. Suckling, and D. Graham, "In situ detection of pterins by SERS," Analyst 134(8), 1561 (2009).
27. H.-J. Van Manen, Y. M. Kraan, D. Roos, and C. Otto, "Single-cell Raman and fluorescence microscopy reveal the association of lipid bodies with phagosomes in leukocytes," Proceedings of the National Academy of Sciences 102(29), 10159–10164 (2005).
28. B. N. Khlebtsov, A. M. Burov, S. V. Zarkov, and N. G. Khlebtsov, "Surface-enhanced Raman scattering from Au nanorods, nanotriangles, and nanostars with tuned plasmon resonances," Physical Chemistry Chemical Physics 25(45), 30903–30913 (2023).
29. N. Pazos-Perez, L. Guerrini, and R. A. Alvarez-Puebla, "Plasmon tunability of gold nanostars at the tip apexes," ACS Omega 3(12), 17173–17179 (2018).
30. G. Frens, "Controlled nucleation for the regulation of the particle size in monodisperse gold suspensions," Nature Physical Science 241(105), 20–22 (1973).
31. B. N. Khlebtsov, A. M. Burov, "Synthesis of monodisperse silica particles by controlled regrowth," Colloid Journal 85(3), 456–468 (2023).
32. V. Tuchin (Ed.), Tissue optics: light scattering methods and instruments for medical diagnostics, 3rd ed., SPIE Press, Bellingham, USA (2015). ISBN: 9781628415162.
33. H. Garn, H. Krause, V. Enzmann, and K. Dröβler, "An improved MTT assay using the electron-coupling agent menadione," Journal of Immunological Methods 168(2), 253–256 (1994).
34. S. M. Thom, R. W. Horobin, E. Seidler, and M. R. Barer, "Factors affecting the selection and use of tetrazolium salts as cytochemical indicators of microbial viability and activity," Journal of Applied Bacteriology 74(4), 433–443 (1993).
35. M. Shoemaker, I. Cohen, and M. Campbell, "Reduction of MTT by aqueous herbal extracts in the absence of cells," Journal of Ethnopharmacology 93(2–3), 381–384 (2004).
36. S.-W. Lim, H.-S. Loh, K.-N. Ting, T. D. Bradshaw, and Z. N. Allaudin, "Reduction of MTT to purple formazan by vitamin e isomers in the absence of cells," Tropical Life Sciences Research 26(1), 111 (2015).
37. L. Peng, B. Wang, and P. Ren, "Reduction of MTT by flavonoids in the absence of cells," Colloids Surfaces B Biointerfaces 45(2), 108–111 (2005).
38. P. Senthil Kumar, I. Pastoriza-Santos, B. Rodríguez-González, F. Javier García de Abajo, and L. M. Liz-Marzán, "High-yield synthesis and optical response of gold nanostars," Nanotechnology 19(1), 015606 (2008).
39. X. Zou, E. Ying, and S. Dong, "Seed-mediated synthesis of branched gold nanoparticles with the assistance of citrate and their surface-enhanced Raman scattering properties," Nanotechnology 17(18), 4758–4764 (2006).
40. J. Xie, Q. Zhang, J. Y. Lee, and D. I. C. Wang, "The synthesis of SERS-active gold nanoflower tags for in vivo applications," ACS Nano 2(12), 2473–2480 (2008).
41. N. G. Khlebtsov, S. V. Zarkov, V. A. Khanadeev, and Y. A. Avetisyan, "A novel concept of two-component dielectric function for gold nanostars: theoretical modelling and experimental verification," Nanoscale 12(38), 19963–19981 (2020).
42. Y. C. Cao, R. Jin, and C. A. Mirkin, "Nanoparticles with Raman spectroscopic fingerprints for dna and rna detection," Science 297(5586), 1536–1540 (2002).

43. J.-M. Nam, C. S. Thaxton, and C. A. Mirkin, "Nanoparticle-based bio-bar codes for the ultrasensitive detection of proteins," Science 301(5641), 1884–1886 (2003).
44. W. E. Doering, S. Nie, "Spectroscopic tags using dye-embedded nanoparticles and surface-enhanced raman scattering," Analytical Chemistry 75(22), 6171–6176 (2003).